AGU PUBLICATIONS

Geophysical Research Letters

Supporting Information for

Dissimilar sensitivities of ocean acidification metrics to anthropogenic carbon accumulation in the Central North Pacific Ocean and California Current Large Marine Ecosystem

Mar C. Arroyo[1], Andrea J. Fassbender[2,3], Brendan R. Carter[4,2], Christopher A. Edwards[1], Jerome Fiechter[1], Addie Norgaard[3,5], and Richard A. Feely[2]

[1]Department of Ocean Sciences, University of California Santa Cruz, Santa Cruz, CA, USA
[2]NOAA/OAR Pacific Marine Environmental Laboratory, Seattle, WA, USA
[3]Monterey Bay Aquarium Research Institute, Moss Landing, CA, USA
[4]Cooperative Institute for Climate, Ocean, and Ecosystem Studies, University of Washington, Seattle, WA, USA
[5]University of Alaska Fairbanks, Fairbanks, AK, USA

Contents of this file

Introduction

This file includes information about the estimation of anthropogenic carbon (C_{anth}) concentrations in the California Current Large Marine Ecosystem (CCLME) and a discussion regarding their uncertainties in Text S1 and Tables S1 and S2. Text S2 provides an additional discussion regarding the methodology for tracking hypercapnia in the CCLME. Fourteen supplementary figures are also included.

Text S1. Anthropogenic Carbon Estimates in the California Current Large Marine Ecosystem

The CCLME anthropogenic carbon (C_{anth}) estimates reported in this study are an update to those in the upper 200 m by Feely et al. (2016). We employ the approach by Carter et al. (2019) – which was focused on basin-scale estimates – with mapping modifications for the coastal environment. Our approach maps reconstructed C_{anth} estimates in the Pacific Ocean by Carter et al. (2019) to the location (longitude, latitude, and depth) of interest in the CCLME using regressions with in situ ocean temperature, salinity, and year as predictors. In contrast to mapping C_{anth} in the open ocean as done by Carter et al. (2019), depth is excluded as a predictor for mapping in the CCLME as seawater properties are more closely related to density (with temperature and salinity collectively serving as a proxy for this property) than water column depth.

This approach represents an improvement over the approach used previously by Feely et al. (2016) due to the larger quantities of C_{anth} estimates used to fit the relationships used to quantify C_{anth}: Feely et al. (2016) fit 2nd order polynomials to C_{anth} estimates from a single zonal (P02) and a single meridional (P16) section intersecting the North American Coast within the CCLME and the Gulf of Alaska, respectively, whereas the new approach uses these sections alongside many additional sections and directly incorporates anthropogenic change estimates obtained from the 2007 to 2016 WCOA cruise occupations (Carter et al., 2019). Despite the change in the methods, the new approach does not yield significantly different C_{anth} estimates on average (Table S1) than either Feely et al.'s (2016) polynomial approach or a direct application of the unmodified regressions outlined by Carter et al. (2019). All approaches seem comparable to within the stated standard uncertainties of ~8 μmol C_{anth} kg^{-1}. Depth-dependent uncertainties in the anthropogenic changes in pH, Ω_{Ar}, pCO_2 and [H$^+$] are shown in Figure S9. These uncertainties are calculated by first propagating the ± 8 μmol kg^{-1} C_{anth} uncertainty in DIC through CO2SYS to estimate the uncertainties in preindustrial pH, Ω_{Ar}, pCO_2 and [H$^+$]. We then compute the difference between the modern, observed parameter and the preindustrial estimated values calculated with and without the ± 8 μmol kg^{-1} C_{anth} uncertainty in DIC. The uncertainties in the anthropogenic changes in pH, Ω_{Ar}, pCO_2 and [H$^+$] are reported using the root-mean-square (RMS) difference between values of all parameters calculated normally (with no C_{anth} uncertainty) and after adding the ± 8 μmol kg^{-1} C_{anth} uncertainty, with the standard deviation of the mean profile each parameter calculated normally and with the ± 8 μmol kg^{-1} C_{anth} uncertainty across all depths in the upper 750 m as a point of reference (Table S2; Figure S9). When the ±8 μmol kg^{-1} uncertainty in individual C_{anth} estimates is propagated through calculations, the depth-dependent uncertainties in ΔpH, $\Delta\Omega_{Ar}$, ΔpCO_2, and Δ[H$^+$] do not change the primary findings of this study (Figure S9). However, the corresponding uncertainty in ΔpCO_2 would influence the volume of water deemed hypercapnic.

Table S1. Average and root mean squared (RMS) differences between the C_{anth} estimation approach used in this study (using WCOA 2016 data) and the approaches used by Feely et al. (2016) polynomial and by the unmodified Carter et al. (2019) for WCOA cruises. ("This study" minus the indicated method, all units are μmol kg^{-1})

Dataset	Average vs. Feely et al. 2016	RMS vs. Feely et al. 2016	Average vs. Carter et al. 2019	RMS vs. Carter et al. 2019
WCOA 2007	-1.3	4.9	-5.6	6.6
WCOA 2011	-3.2	6.1	-5.6	6.3
WCOA 2012	-3.9	6	-5.5	6.2
WCOA 2013	-4.1	6.4	-6.7	7.4
WCOA 2016	-4.9	7.3	-6.1	6.9

Table S2. The root-mean-squared (RMS) difference between the anthropogenic changes (Δ) in pH, Ω_{Ar}, pCO_2, and $[H^+]$ calculated with and without the ± 8 μmol kg^{-1} uncertainty in C_{anth} and the standard deviation of the mean profile of parameters with and assuming no C_{anth} uncertainty in the upper 750 m.

Parameter	RMS vs. -8 μmol kg^{-1} C_{anth}	RMS vs. +8 μmol kg^{-1} C_{anth}	
ΔpH	0.021	0.021	
$\Delta\Omega_{Ar}$	0.067	0.068	
ΔpCO_2	37 μatm	34 μatm	
$\Delta[H^+]$	0.66 nmol kg^{-1}	0.62 nmol kg^{-1}	
Parameter	**Standard Deviation (-8 μmol kg^{-1} C_{anth})**	**Standard Deviation (+8 μmol kg^{-1} C_{anth})**	**Standard Deviation (no C_{anth} uncertainty)**
ΔpH	0.020	0.017	0.018
$\Delta\Omega_{Ar}$	0.157	0.181	0.169
ΔpCO_2	55 μatm	85 μatm	70 μatm
$\Delta[H^+]$	0.99 nmol kg^{-1}	1.55 nmol kg^{-1}	1.26 nmol kg^{-1}

Text S2. Tracking hypercapnic events in the CCLME

In this study, we define hypercapnic conditions in waters with in situ pCO_2 values greater than or equal to 1000 µatm, following thresholds set by the prior studies of McNeil & Sasse (2016) and Feely et al., (2018). However, many other definitions for the hypercapnic thresholds exist in current literature. For example, Esbaugh et al. (2012) found hypercapnia effects on the acid-base balance of adult Gulf toadfish with pCO_2 levels as low as 750 µatm. Other studies find detrimental effects occur in fishes when pCO_2 values exceed a concentration threshold over a certain exposure time. Nilsson et al. (2012) found loss of behavior lateralization (e.g., preferred direction of turning) occurred in larval coral reef fishes exposed to pCO_2 levels of ~900 µatm for 4 days. Though the exact definition of hypercapnia may vary, a review by Heuer & Grosell (2014) discuss that many sublethal effects on marine fishes may occur when pCO_2 values range from 500 to 25000+ µatm at different life stages, suggesting that 1000 µatm is a realistic (while somewhat arbitrary) threshold to contextualize ecological harm. These effects of elevated pCO_2 levels include impacts to neurosensory behavior (e.g., activity levels) as well as the growth and development of certain species (see their Figure 2). We acknowledge that our definition of hypercapnia ($pCO_2 \geq 1000$ µatm) may not apply to all marine organisms. A key point of our study is to emphasize that the largest C_{anth}-driven changes in pCO_2 (and $[H^+]$) occur well below the surface in the mesopelagic, while the largest C_{anth}-driven changes in pH and Ω_{Ar} are more localized to the upper ~150 m of the water column in the CCLME. We build off previous research from this region to discuss hypercapnia as an additional modern stressor to mid-water organisms. Additionally, the mesopelagic zone is where dissolved oxygen levels are naturally low, leading to the compounding effect of low dissolved oxygen and high pCO_2 that make it difficult for organisms to breathe and respire.

To estimate hypercapnic events in the CCLME, we tracked the average observed minimum hypercapnic density surface during WCOA 2016 (Figure S3) in daily output from a near real-time model in the CCLME between 2011 and 2020. We define an event when this average density surface is shallower than the 200 m isobath (approximate shelf break) on a given day. For example, if the density surface oscillates around the 200 m isobath during the transition from non-upwelling to upwelling conditions over the course of several days, each daily crossing of the 200 m isobath will be categorized as a distinct daily event instead of as oscillations of the same event. Though this may lead to a slight overestimation on the number of hypercapnic events each year, we report the average maximum duration when events occur at a given latitude (Figure 4b) to show how long events may persist at the 200 m isobath. Additionally, we report regional averages for northern, central, and southern subregions of the CCLME. However, regional averaging might not be representative for every location within each subregion because there are certain locations that are hotspots for hypercapnic events (see Figures S10 and S11). In the real coastal ocean, the presence of subsurface hypercapnic water on the continental shelf will depend on the local bathymetry and coastal topography of the region. These spatial features may not be fully resolved in the relatively coarse CCLME NRT model. In this study, we use the CCLME NRT model bathymetry to determine the location (latitude and longitude) of the 200 m isobath for internal consistency within the modelling framework, despite differences between this model and the higher resolution gridded bathymetric data from the General Bathymetric Chart of the Oceans (GEBCO; Figure S1b).

Further, model results within ~0.5 to 1° of the CCLME NRT domain boundary may be subjected to uncertainties attributed to boundary conditions. We neglect hypercapnic events that occur within 0.5° of the CCLME NRT latitudinal bounds in the event analysis to account for these biases.

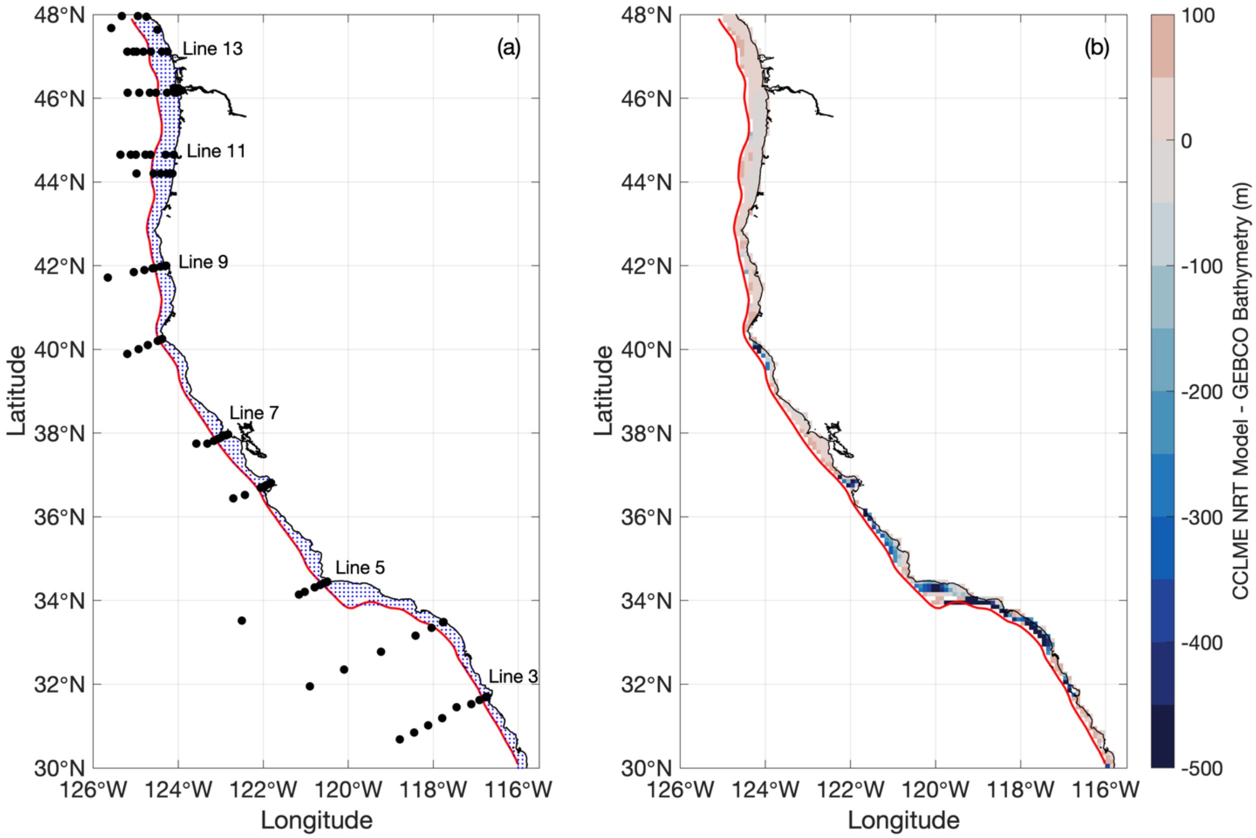

Figure S1. (**a**) Observational and near real-time (NRT) model domain in the CCLME. Black dots indicate the sampling stations from various cross-shelf transects during WCOA 2016. The red line indicates the continental shelf boundary at the 200 m isobath and blue dots indicate the model grid points on the continental shelf. (**b**) Differences between CCLME NRT model and GEBCO bathymetry (m).

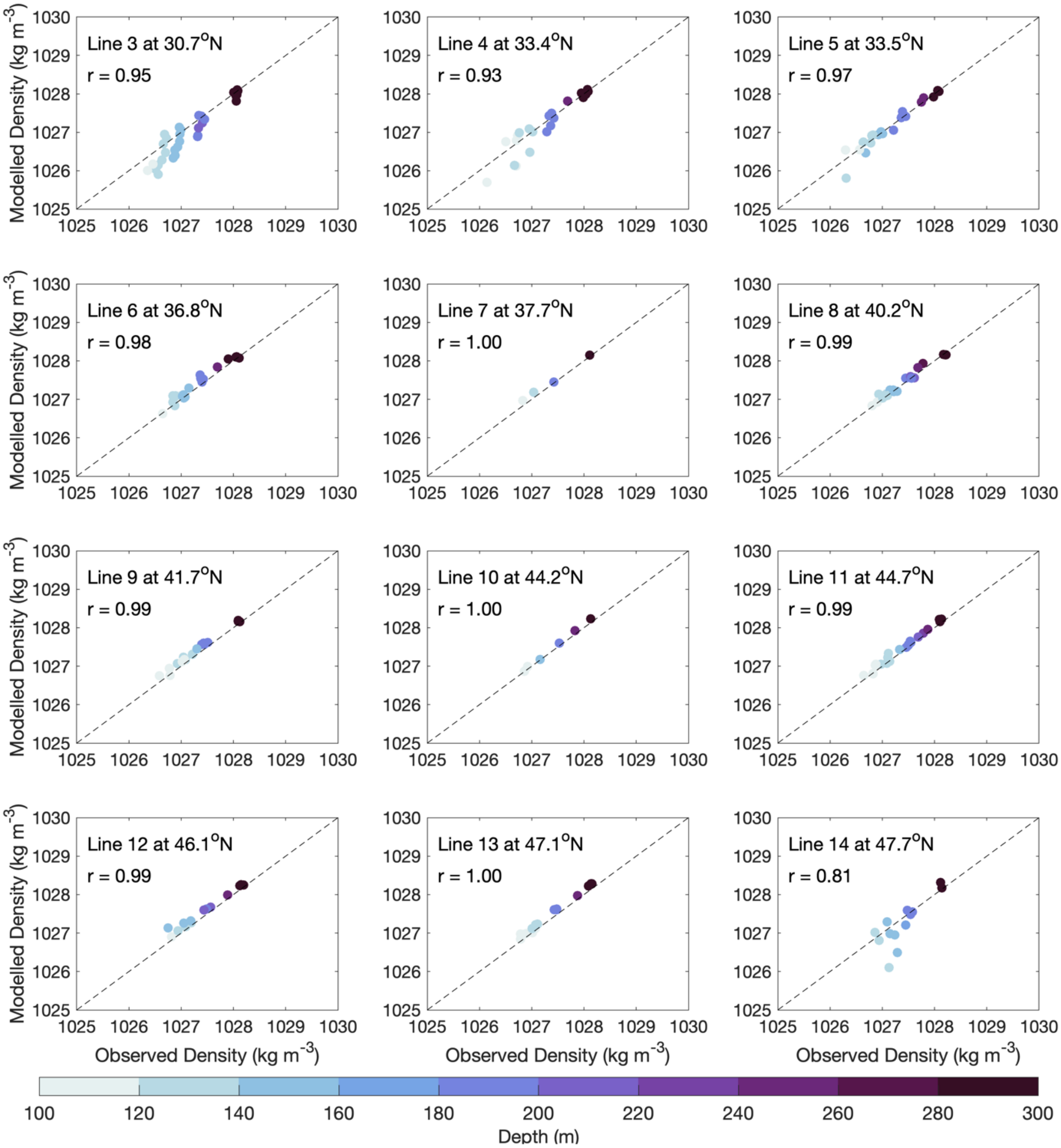

Figure S2. Comparison of WCOA 2016 observations and simultaneous (by day) CCLME NRT 2016 simulations of density (kg m^{-3}) at stations sampled along each cruise transect (Lines 3 to 14; see Figure S1a) between 100 and 300 m (colors), enveloping the depth range of the observed upper density of hypercapnia (see Figure S3). In each panel, the 1:1 line (dashed) is shown, and the Pearson's correlation coefficient (r) for each cruise transect is indicated in the upper left corner.

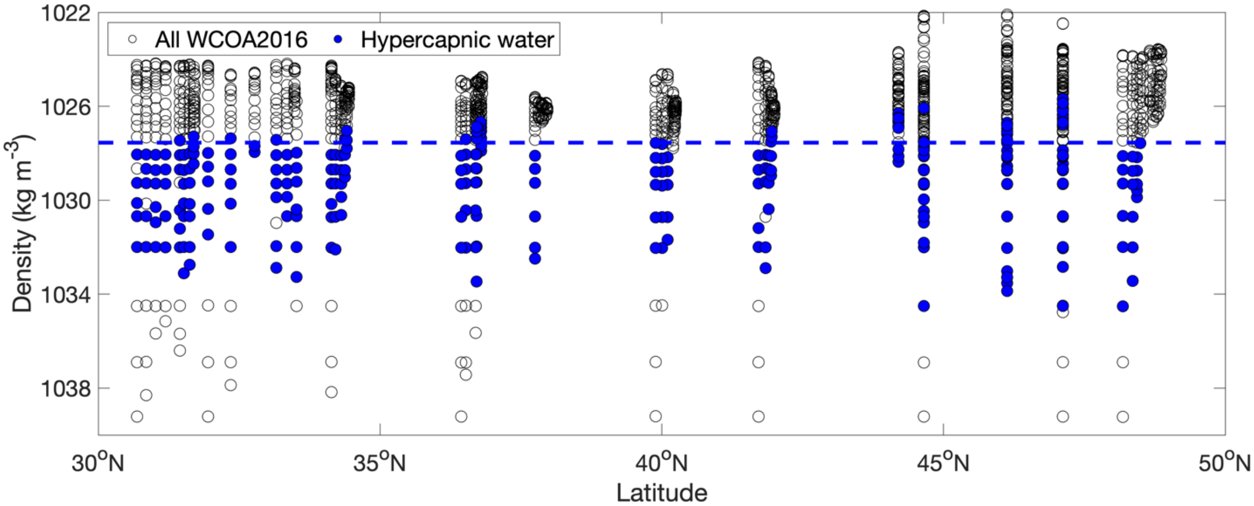

Figure S3. Observed densities (kg m^{-3}) on which hypercapnia (blue; pCO$_2$ ≥ 1000 µatm) occurred during the WCOA 2016 cruise (all circles) from samples collected within the CCLME NRT model domain (30°N-48°N). The blue dashed line represents the observed average minimum density for hypercapnia (1027.5 kg m^{-3}) that was tracked in the CCLME NRT physical model simulations to estimate occurrence of hypercapnic events.

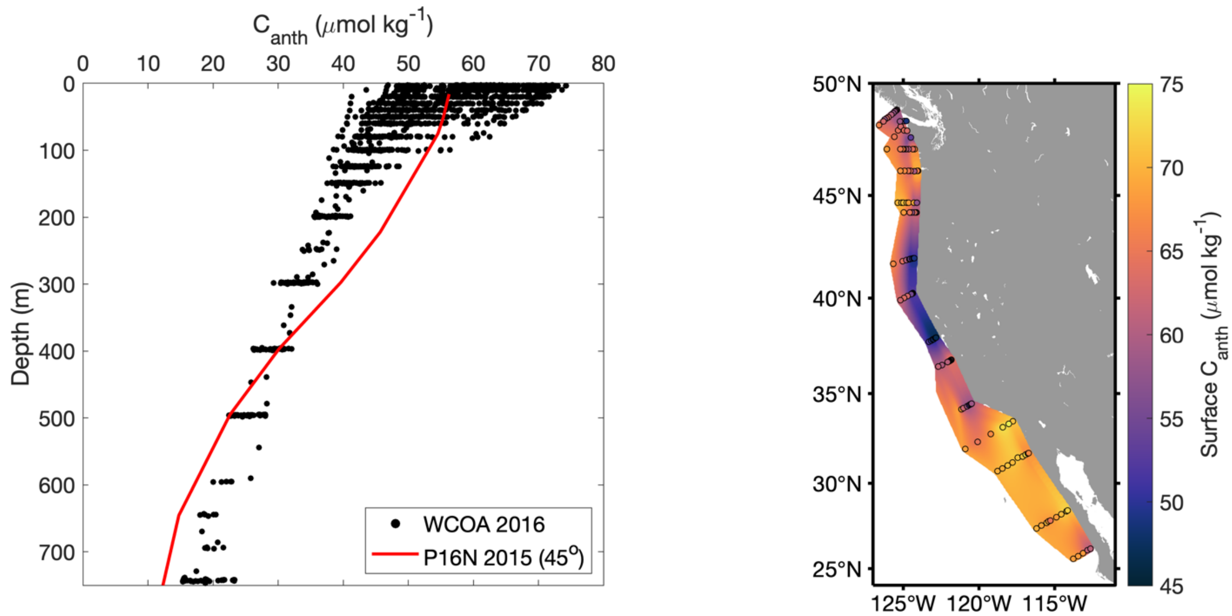

Figure S4. (**a**) Estimates of anthropogenic carbon (C_{anth}, µmol kg^{-1}) in the upper 750 m at WCOA 2016 cruise stations in the CCLME (black dots) and at 45°N, ~152°W in the North Pacific Ocean (red) from Carter et al. (2017). (**b**) Surface distribution of C_{anth} during WCOA 2016, interpolated from surface observations (circles).

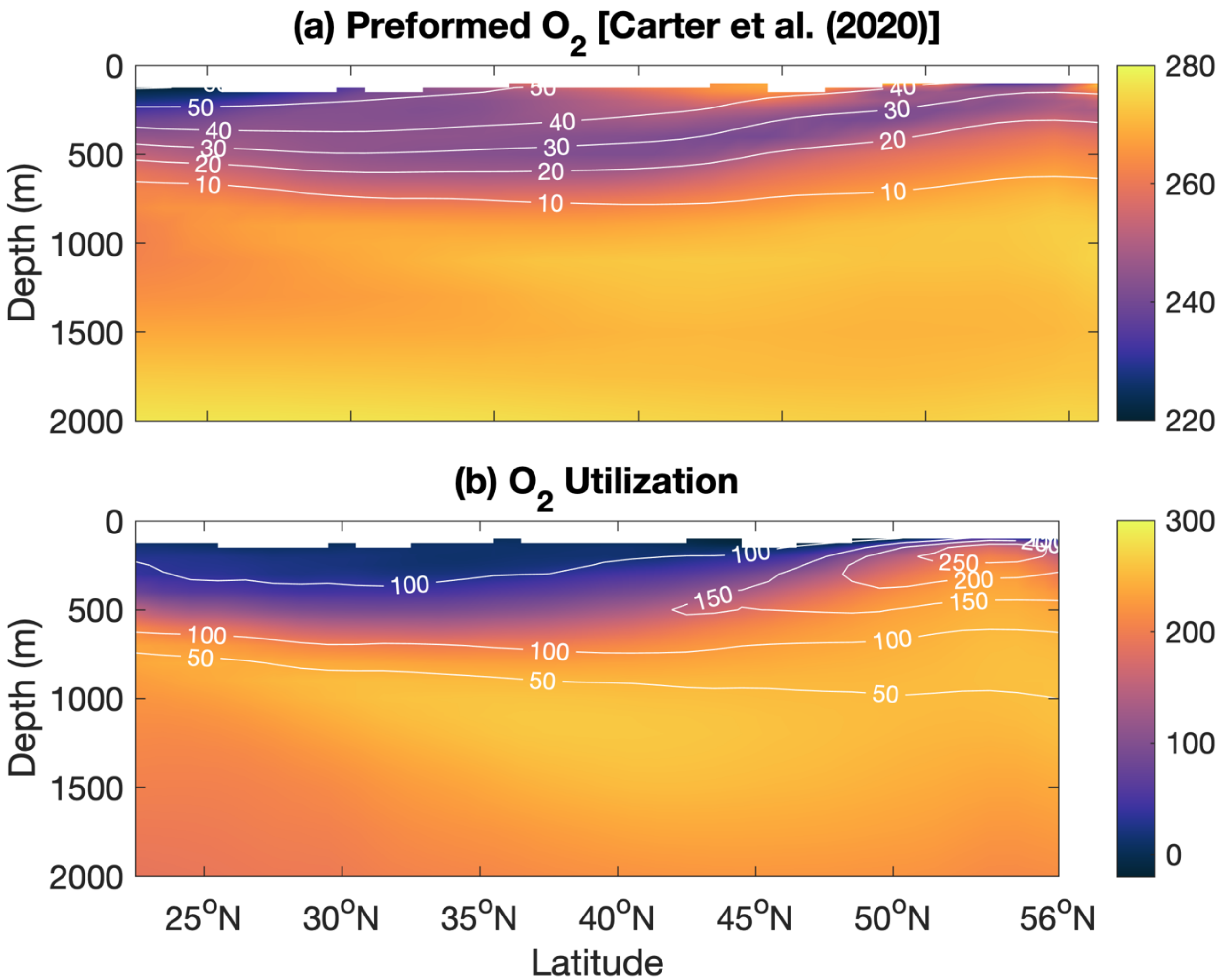

Figure S5. (**a**) Preformed dissolved oxygen (μmol kg^{-1}) from Carter et al. (2020) and (**b**) the utilization of dissolved oxygen (μmol kg^{-1}) based on the difference between preformed O_2 from Carter et al. (2020) and observed O_2 from GLODAPv2 2016 (Lauvset et al. 2016) in the Central North Pacific Ocean along ~152°N between 22.5°N and 56°N. White contours in (**a**) show anthropogenic carbon (μmol kg^{-1}) values through the year 2002 from GLODAPv2, and white contours in (**b**) show the change in pCO$_2$ (modern pCO$_2$ – preindustrial pCO$_2$; μatm) due to anthropogenic carbon accumulation.

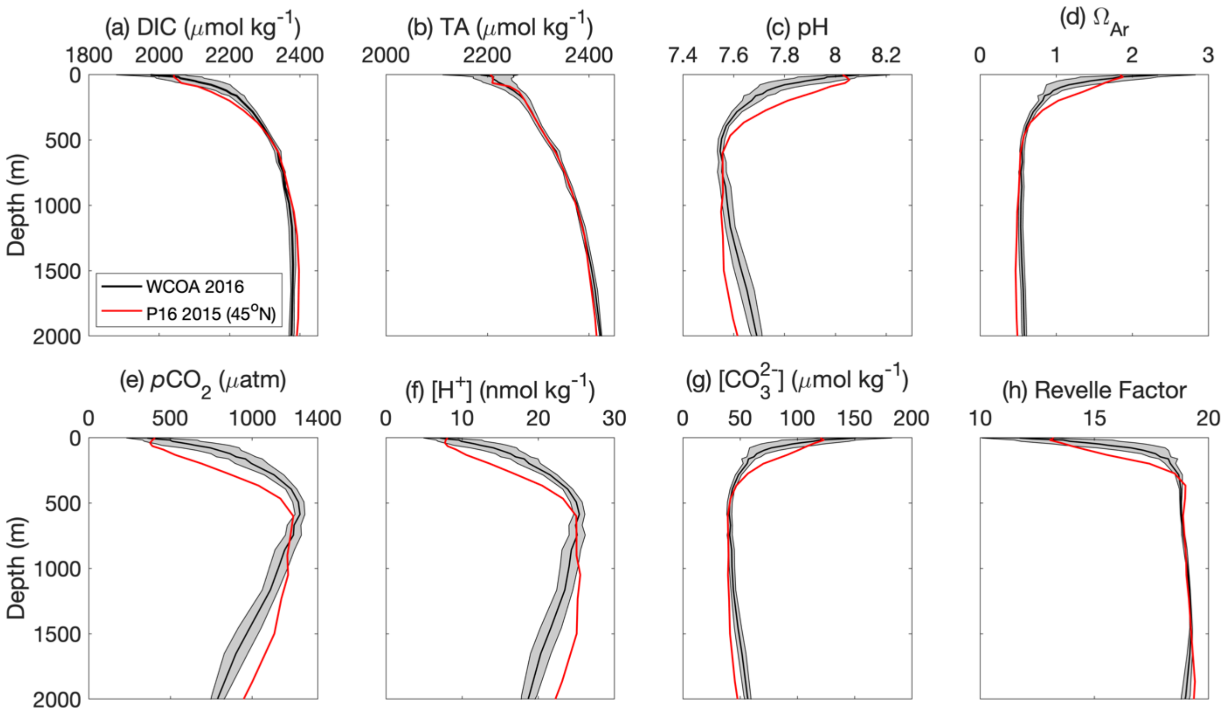

Figure S6. Profiles of carbonate system parameters in the open and coastal North Pacific Ocean. Mean (black) and one standard deviation (gray) profiles during the WCOA 2016 cruise in the CCLME and at 45°N, ~152°W from CLIVAR/GO-SHIP P16N in 2015 (red) for: (**a**) DIC (μmol kg^{-1}), (**b**), TA (μmol kg^{-1}), (**c**) pH on the total scale, (**d**) aragonite saturation state (Ω_{Ar}), (**e**) pCO_2 (μatm), (**f**) $[H^+]$ (nmol kg^{-1}), (**g**) $[CO_3^{2-}]$ (μmol kg^{-1}), and (**h**) Revelle Factor.

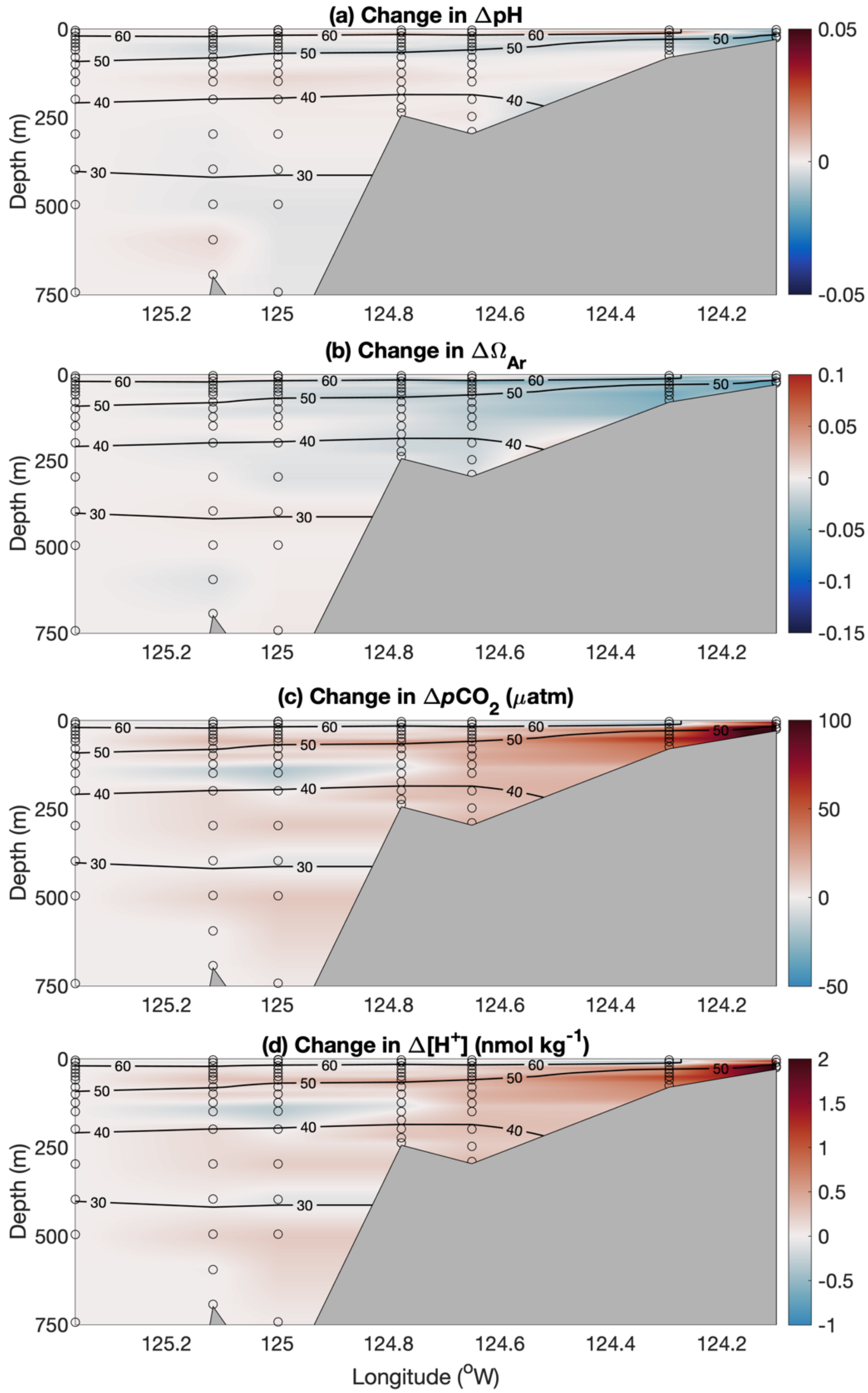

Figure S7. Changes in carbonate system parameters along density surfaces from offshore to onshore at Line 11 (~45°N; Figure S1a) in the CCLME as a metric for enhanced remineralization over the continental shelf. The furthest offshore value was subtracted from all values on the same density surface for (**a**) ΔpH, (**b**) $\Delta\Omega_{Ar}$, (**c**) ΔpCO_2 (µatm), and (**d**) $\Delta[H^+]$ (nmol kg^{-1}) where Δ = modern - preindustrial. Contours show concentrations of anthropogenic carbon (C_{anth}; µmol kg^{-1}).

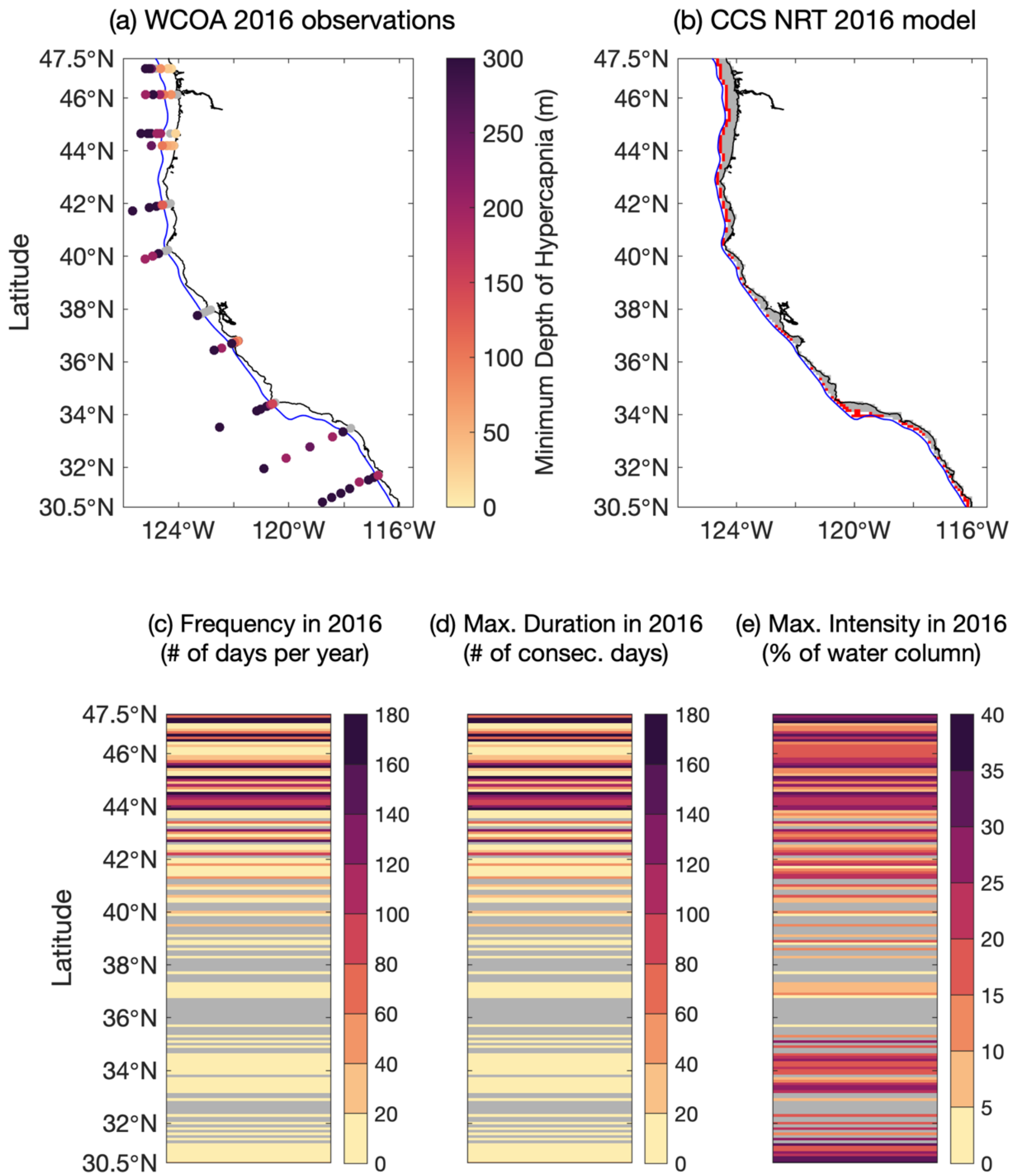

Figure S8. Hypercapnia in the CCLME in 2016. (**a**) Observed minimum depth (m) of hypercapnia at sampling stations during WCOA 2016. (**b**) The simulated locations (red) of hypercapnia on the shelf in 2016 estimated by the CCLME NRT model, determined by tracking the minimum hypercapnic density (see methods). In (**a**) and (**b**), gray indicates no hypercapnia occurrence (observed or simulated), and the blue line delineates the 200 m isobath. The simulated (**c**) frequency, (**d**) maximum duration, and (**e**) maximum intensity of hypercapnic events at the 200 m isobath in 2016. Gray indicates no hypercapnic event occurred. See main text for metric definitions.

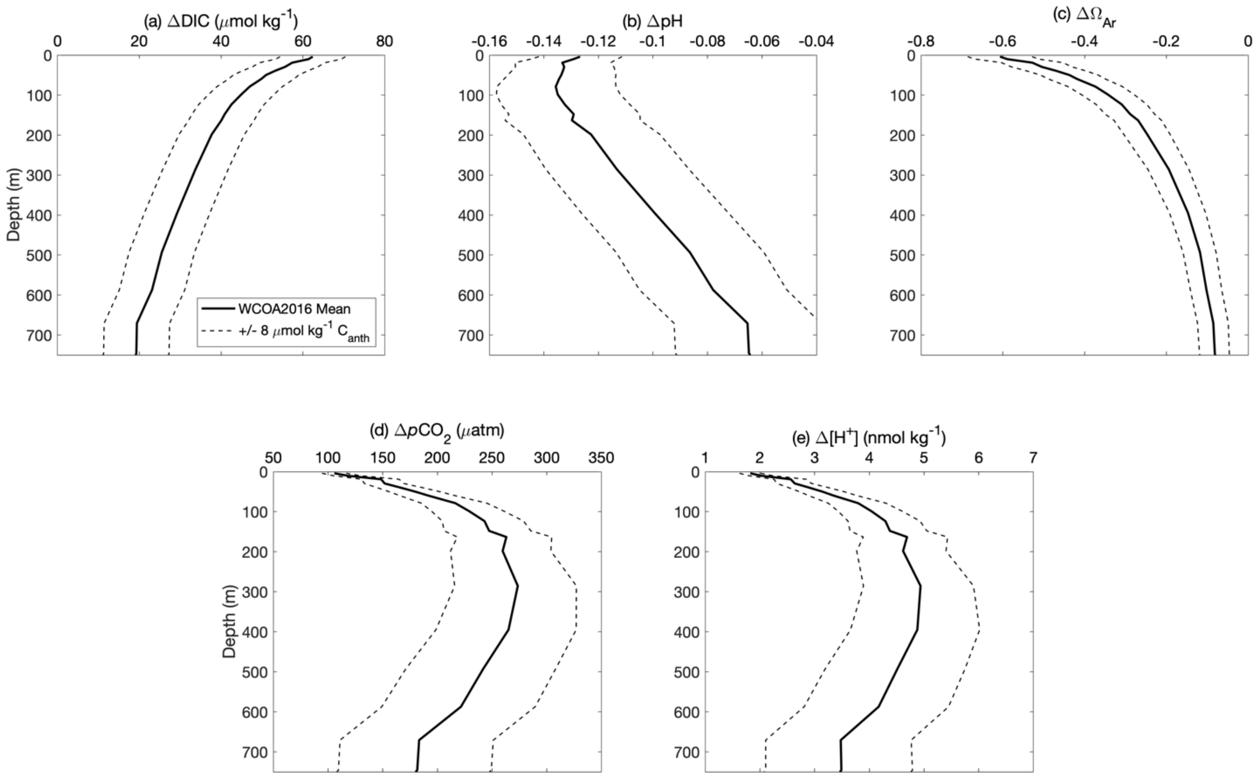

Figure S9. Depth-dependent uncertainties in (**a**) ΔDIC, (**b**) ΔpH, (**c**) $\Delta\Omega_{Ar}$, (**d**) $\Delta p CO_2$, and (**e**) $\Delta[H^+]$ in the upper 750 m in the CCLME. The bold line in each figure represents the average profile from all CCLME stations, as in Figure 2 of the main text. The dashed lines represent the average profiles of parameters when the ±8 μmol kg^{-1} uncertainty in individual C_{anth} estimates is propagated through calculations (see Text S2 and Table 2).

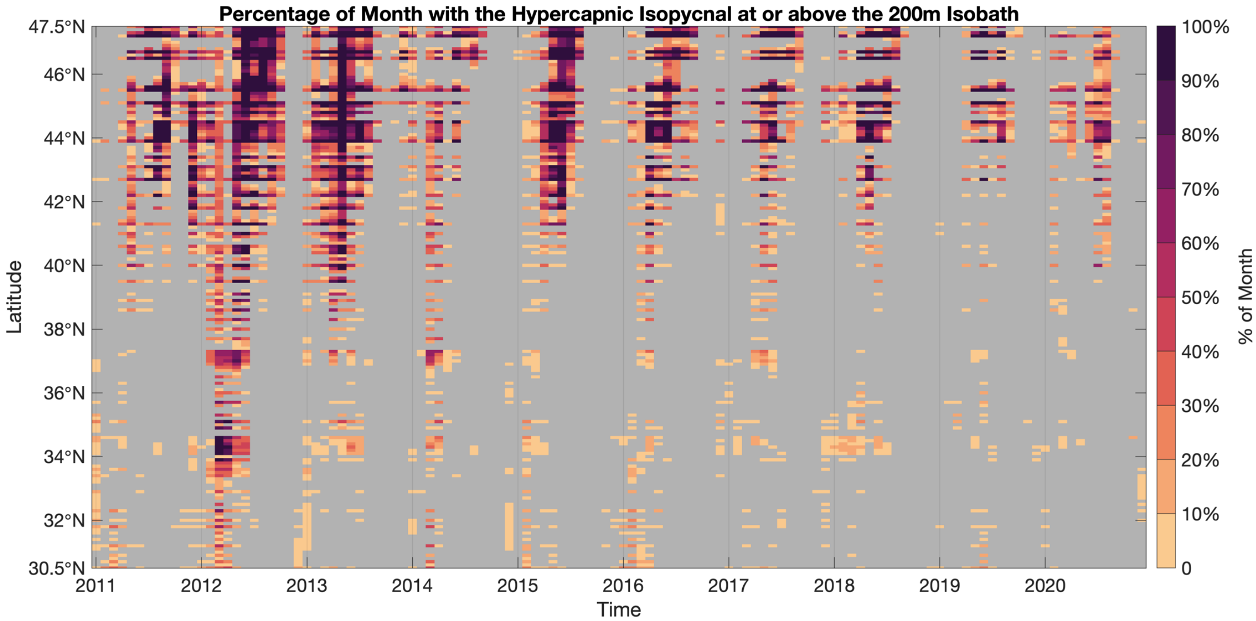

Figure S10. Percentage of the month when the hypercapnic isopycnal was at or above the 200 m isobath for months between 2011 and 2020 in the CCLME NRT model. Gray indicates no hypercapnic event occurred at the 200 m isobath.

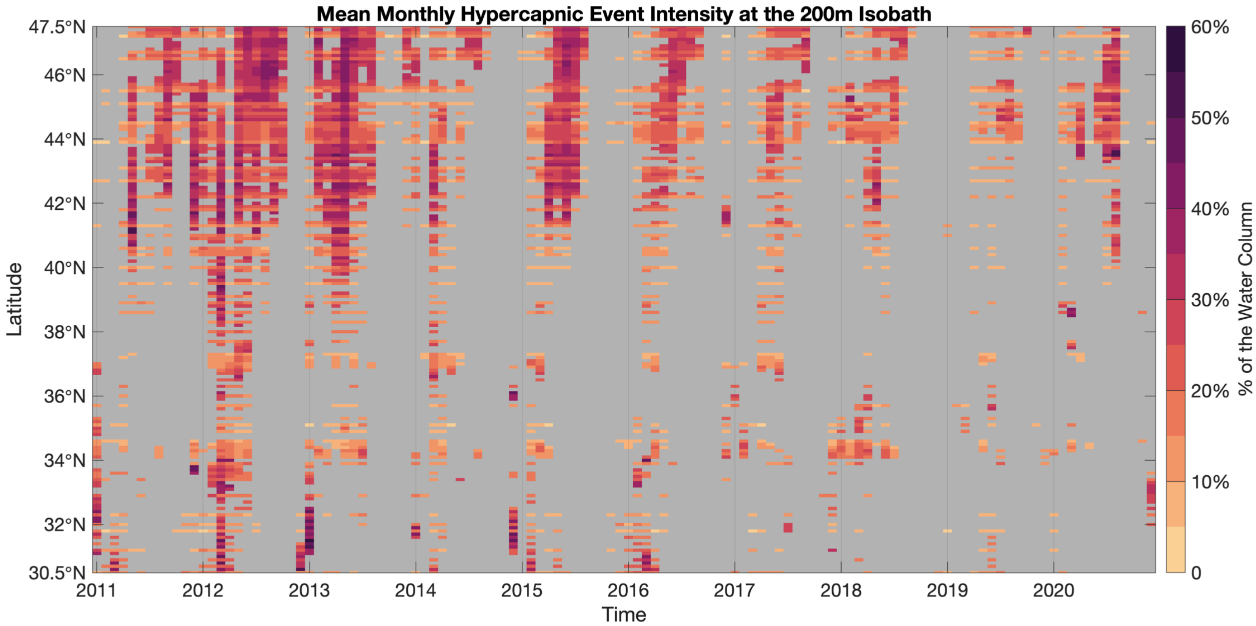

Figure S11. Mean monthly hypercapnic intensity at the 200 m isobath for events that occurred during between 2011 and 2020 in the CCLME NRT model. Gray indicates no hypercapnic event occurred at the 200 m isobath.

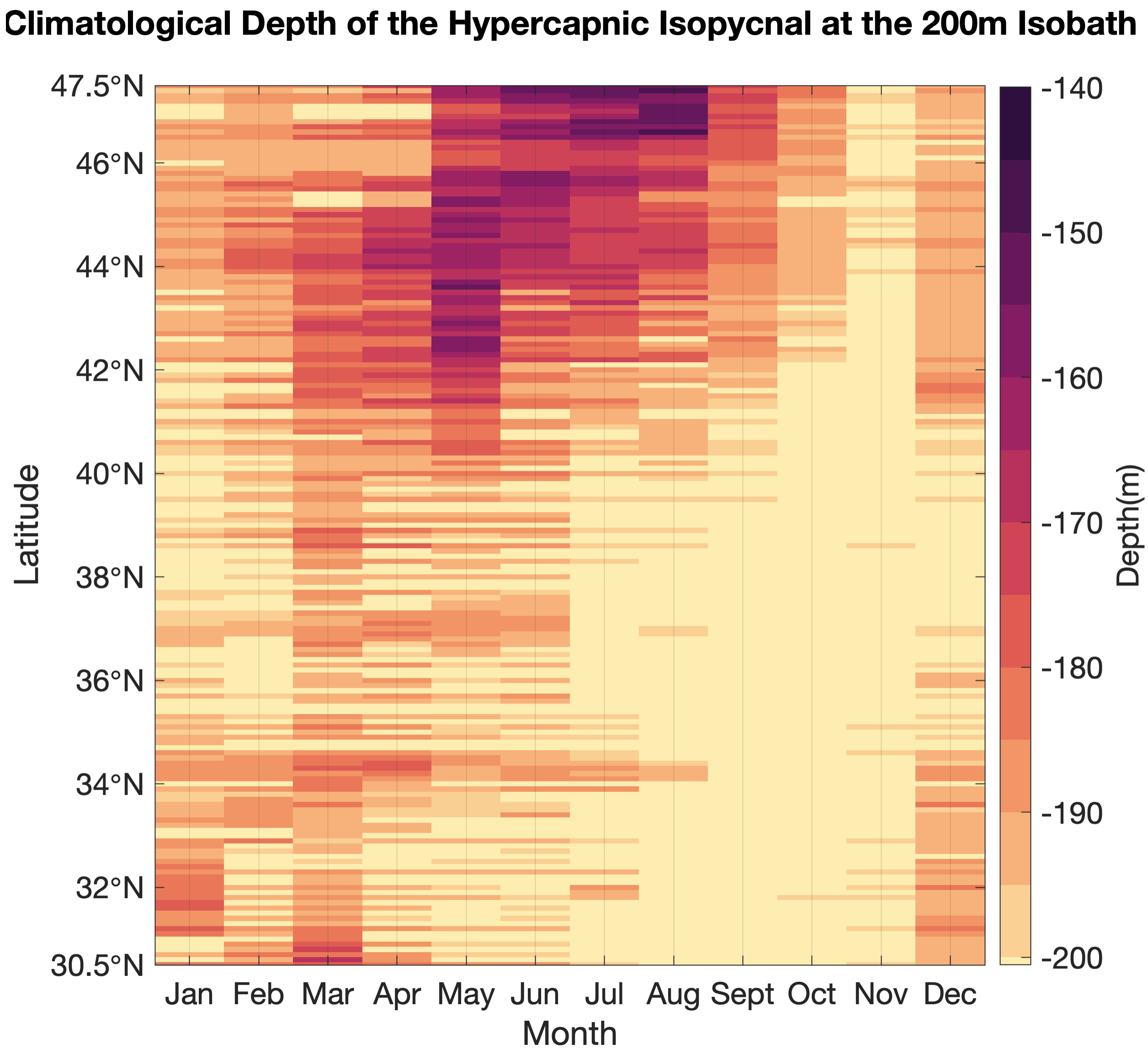

Figure S12. Climatological mean depth of the hypercapnic isopycnal at the 200 m isobath. The climatology was calculated by taking the average across months of the mean monthly hypercapnic isopycnal depth between 2011 and 2020 in the CCLME NRT model and assuming a mean monthly isopycnal depth of 200 m when no event occurred.

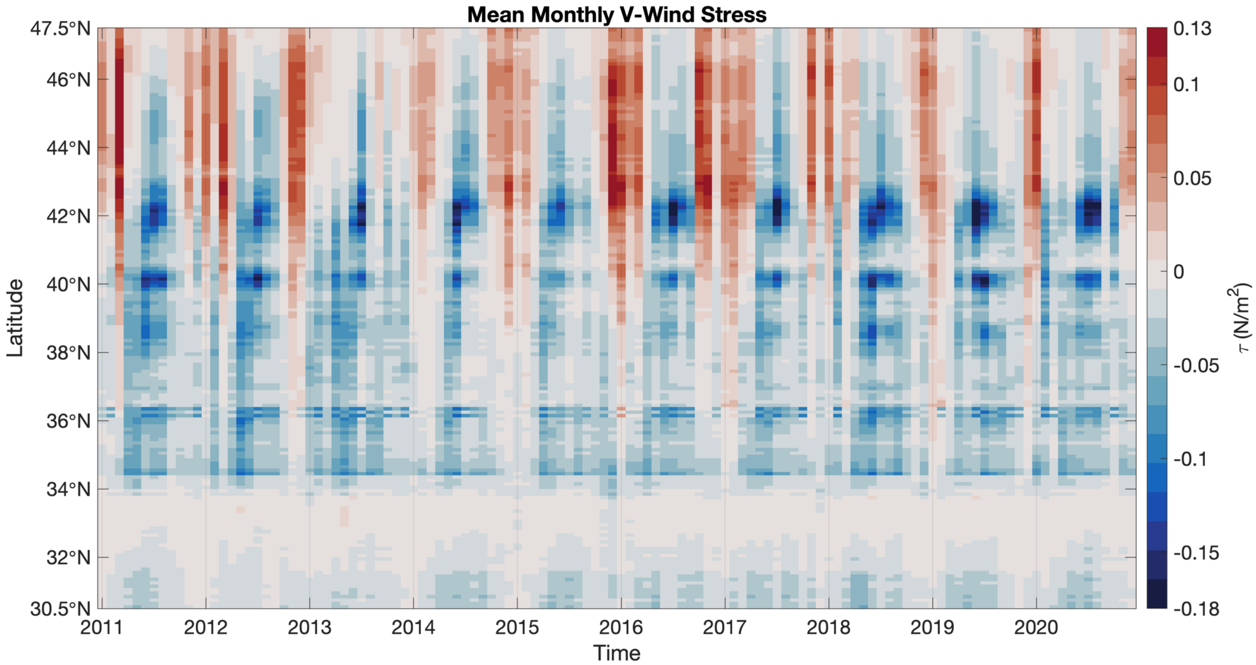

Figure S13. Mean monthly v-wind stress (τ; N/m^2) averaged longitudinally between the coast and the 200 m isobath for months between 2011 and 2020 in the CCLME NRT model.

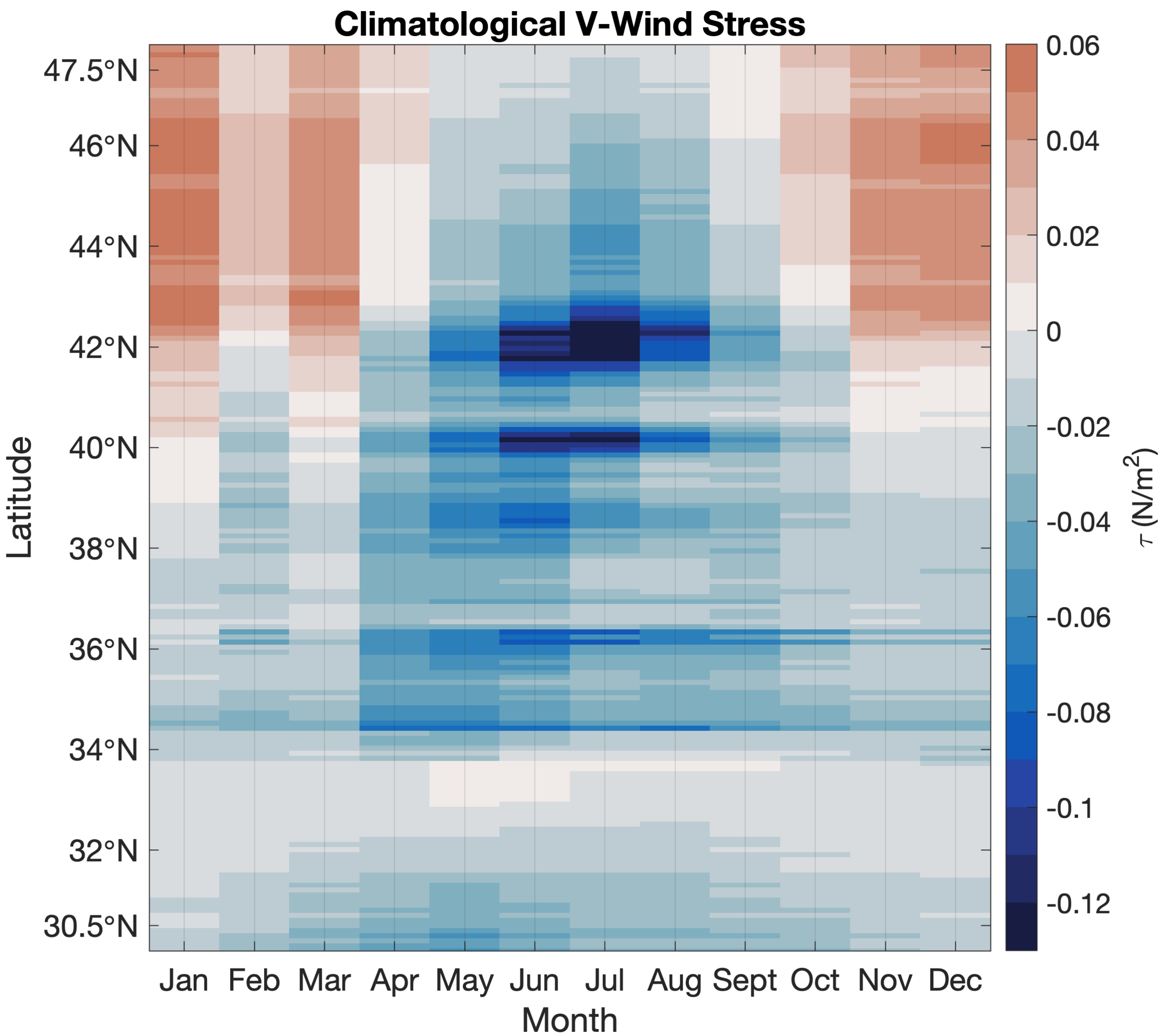

Figure S14. Climatological monthly mean v-wind stress (τ; N/m^2) averaged longitudinally between the coast and the 200 m isobath for months between 2011 and 2020 in the CCLME NRT model.

Supporting References

Carter, B. R., Feely, R. A., Lauvset, S. K., Olsen, A., DeVries, T., & Sonnerup, R. (2020). Preformed Properties for Marine Organic Matter and Carbonate Mineral Cycling Quantification. *Global Biogeochemical Cycles, 35*, e2020GB006623. https://doi.org/10.1029/2020GB006623

Carter, B. R., Feely, R. A., Mecking, S., Cross, J. N., Macdonald, A. M., Siedlecki, S. A., et al. (2017). Two decades of Pacific anthropogenic carbon storage and ocean acidification along Global Ocean Ship-based Hydrographic Investigations Program sections P16 and P02. *Global Biogeochemical Cycles, 31*, 306-327. https://doi.org/10.1002/2016GB005485

Carter, B. R., Feely, R. A., Wanninkhof, R., Kouketsu, S., Sonnerup, R. E., Pardo, P. C., et al. (2019). Pacific Anthropogenic Carbon Between 1991 and 2017. *Global Biogeochemical Cycles*, *33*(5), 597–617. https://doi.org/10.1029/2018GB006154

Esbaugh, A. J., Heuer, R., & Grosell, M. (2012). Impacts of ocean acidification on respiratory gas exchange and acid–base balance in a marine teleost, Opsanus beta. *Journal of Comparative Physiology B*, *182*(7), 921–934. https://doi.org/10.1007/s00360-012-0668-5

Feely, R. A., Alin, S. R., Carter, B., Bednaršek, N., Hales, B., Chan, F., et al. (2016). Chemical and biological impacts of ocean acidification along the west coast of North America. *Estuarine, Coastal and Shelf Science*, *183*, 260–270. https://doi.org/10.1016/j.ecss.2016.08.043

Feely, R. A., Okazaki, R. R., Cai, W. J., Bednaršek, N., Alin, S. R., Byrne, R. H., & Fassbender, A. (2018). The combined effects of acidification and hypoxia on pH and aragonite saturation in the coastal waters of the California current ecosystem and the northern Gulf of Mexico. *Continental Shelf Research*, *152*, 50–60. https://doi.org/10.1016/j.csr.2017.11.002

Heuer, R. M., & Grosell, M. (2014). Physiological impacts of elevated carbon dioxide and ocean acidification on fish. *American Journal of Physiology - Regulatory Integrative and Comparative Physiology*, *307*(9), R1061–R1084. https://doi.org/10.1152/ajpregu.00064.2014

Lauvset, S. K., Key, R. M., Olsen, A., Van Heuven, S., Velo, A., Lin, X., et al. (2016). A new global interior ocean mapped climatology: The 1° × 1° GLODAP version 2. *Earth System Science Data*, *8*(2), 325–340. https://doi.org/10.5194/essd-8-325-2016

McNeil, B. I., & Sasse, T. P. (2016). Future ocean hypercapnia driven by anthropogenic amplification of the natural CO_2 cycle. *Nature*, *529*(7586), 383–386. https://doi.org/10.1038/nature16156

Nilsson, G. E., Dixson, D. L., Domenici, P., McCormick, M. I., Sørensen, C., Watson, S. A., & Munday, P. L. (2012). Near-future carbon dioxide levels alter fish behaviour by interfering with neurotransmitter function. *Nature Climate Change*. https://doi.org/10.1038/nclimate1352